Direct observation of double-***k*** lattice modulation in double-***k*** magnetic structures. The case of $CeAl_2$

2009 J. Phys.: Condens. Matter 21 376004

(http://iopscience.iop.org/0953-8984/21/37/376004)

IOP PUBLISHING JOURNAL OF PHYSICS: CONDENSED MATTER

J. Phys.: Condens. Matter **21** (2009) 376004 (12pp) doi:10.1088/0953-8984/21/37/376004

Direct observation of double-k lattice modulation in double-k magnetic structures. The case of $CeAl_2$

A Stunault[1,6], J Schweizer[2], F Givord[2,7], C Vettier[3,4], C Detlefs[3], J-X Boucherle[2,7,8] and P Lejay[5]

[1] Institut Laue Langevin, BP156, 38042 Grenoble Cedex 9, France
[2] CEA-Grenoble, DSM/INAC/SPSMS/MDN, 38054 Grenoble Cedex 9, France
[3] European Synchrotron Radiation Facility, BP 220, 38043 Grenoble Cedex 9, France
[4] European Spallation Source—Scandinavia (ESSS), PO BOX 117, SE-221 00 Lund, Sweden
[5] Institut Néel, CNRS, BP166, 38042 Grenoble Cedex 9, France

E-mail: stunault@ill.fr

Received 2 June 2009, in final form 31 July 2009
Published 21 August 2009
Online at stacks.iop.org/JPhysCM/21/376004

Abstract

Symmetry analysis is combined with x-ray scattering experiments to investigate the lattice modulation associated with the incommensurate magnetic structure in the case of a double-$\boldsymbol{k}$ structure. The expansion of the free energy shows that the components of the magnetic structure with propagation vectors $\boldsymbol{k_1}$ and $\boldsymbol{k_2}$ can couple via components of lattice modulations. It is shown that the classical diffraction peaks reflecting a $2\boldsymbol{k}$ propagation vector, associated with magneto-elastic effects in single-$\boldsymbol{k}$ structures, will coexist with diffraction peaks with propagation vectors $\boldsymbol{k_1} - \boldsymbol{k_2}$ or $\boldsymbol{k_1} + \boldsymbol{k_2}$. The existence of these latter peaks can be considered as a signature of a double-$\boldsymbol{k}$ magnetic structure. In the case of the double-$\boldsymbol{k}$ modulated structure of $CeAl_2$, group theory is applied directly to the study of the charge modulation. An x-ray scattering study of the $2\boldsymbol{k}$ satellites shows that the lattice displacements of the two Ce sites of the structure are antiparallel to each other, and perpendicular to the direction of the magnetic modulation. We also confirm experimentally the existence of $\boldsymbol{k_1} + \boldsymbol{k_2}$ satellites.

(Some figures in this article are in colour only in the electronic version)

1. Introduction

In the past 50 years, a large number of complex magnetic structures have been solved using neutron diffraction or, more recently, resonant x-ray magnetic scattering. Among these are all kinds of non-collinear structures, as well as incommensurate or multi-$\boldsymbol{k}$ structures. The determination of the magnetic structure often requires the combination of scattering experiments and symmetry considerations, particularly in the case of non-collinear structures. Based on the Landau theory of second order transitions, symmetry analysis may be applied to magnetic structure resulting from a second order magnetic phase transition. With the help of group theory, it constitutes a powerful tool which allows one to establish relationships between the Fourier components of the magnetic moments, and to determine the possible magnetic structures allowed by the crystal symmetry.

The onset of magnetic order can lead to magnetostriction effects which in turn induce the onset of charge modulation in the material [1]. Conceptually, there are two mechanisms for producing a density wave in the charge distribution. First, the lattice may be periodically distorted, with each ion retaining its equilibrium charge (strain wave). Second, there may be a periodic excess and deficit of charge on the sites of an undistorted lattice. In the literature, these two effects are collectively referred to as charge density wave (CDW). We may note here that the dominant contribution to the x-ray intensities arises from the core electrons (the strain wave). In chromium, strain wave effects (modulation of the atomic positions) and

[6] Author to whom any correspondence should be addressed.
[7] CNRS staff.
[8] Present address: dr11, CNRS, BP166, 38042 Grenoble Cedex 9, France.

CDW effects (modulation of the charge distribution) could be separated [2]. Such a distinction is beyond the scope of the present paper. Here, only strain waves (lattice distortions) will be considered.

The magnetostrictive interactions, and therefore the corresponding displacements, are invariant in a general reversal of the moments and, for a simple, single-$\boldsymbol{k}$ magnetic structure, the period of the charge modulation is half the period of the magnetic modulation, resulting in propagation vectors $2\boldsymbol{k}$. This feature has been thoroughly studied e.g. in chromium, using neutrons or x-rays [3–5] and can provide a very convenient tool for the study of magnetic domain populations [6], or magnetic propagation vectors [7, 8]. In the case of a double-$\boldsymbol{k}$ magnetic structure, we will show that components of the displacements are also expected, which couple both propagation vectors of the magnetic structure and give rise to satellite reflections with a propagation vector $\boldsymbol{k_1} \pm \boldsymbol{k_2}$. Observations of such effects have been reported in UAs [9].

Similarly to what is done in the determination of a magnetic structure, symmetry analysis can be applied to the study of a lattice modulation, to establish relationships between the Fourier components of the atomic displacements. As an application, we consider the double-$\boldsymbol{k}$ modulated structure of $CeAl_2$. The Kondo compound $CeAl_2$ crystallizes in the $MgCu_2$ cubic Laves phase (space group O_h^7), with two Ce sites, Ce_1 and Ce_2, at positions (1/8, 1/8, 1/8) and (−1/8, −1/8, −1/8). It orders antiferromagnetically at low temperature ($T_N = 3.8$ K). The magnetic structure is a rather complex double-$\boldsymbol{k}$ structure with propagation vectors of type $(1/2 + \delta, 1/2 - \delta, 1/2)$, with $\delta = 0.112$ [11]. The 12 propagation vectors of the star of $\boldsymbol{k}$ couple in pairs, like e.g. $\boldsymbol{k_1} = (1/2 + \delta, 1/2 - \delta, 1/2)$ and $\boldsymbol{k_2} = (1/2 + \delta, 1/2 - \delta, -1/2)$, which gives rise to 6 $\boldsymbol{k}$-domains. Coupled propagation vectors are the sum of the same modulation part, e.g. $(+\delta, -\delta, 0)$ and two different antiferromagnetic parts, e.g. (1/2, 1/2, 1/2) and (1/2, 1/2, −1/2), perpendicular to the modulation part. The Fourier components $\boldsymbol{m}^{k_1}$ and $\boldsymbol{m}^{k_2}$ are in phase quadrature and are aligned almost along the [1 1 1] and [1 1 $\bar{1}$] diagonals, respectively [12, 13]. There is also a phase difference between the x, y and z components of each of the Fourier components $\boldsymbol{m}^{k_1}$ and $\boldsymbol{m}^{k_2}$. With these features, the Ce_1 and Ce_2 sublattices order in elliptical helices. The helix axes are parallel to the modulated part of the propagation vector, and the cerium moments are slightly tilted away from the planes of the ellipses [14].

While previous work was devoted to an ever better understanding of the magnetic structure of $CeAl_2$ [11–15], the present paper deals with the associated magneto-elastic distortion, first through a theoretical approach, via group theory considerations, then from the experimental point of view, using synchrotron x-ray scattering. The scope of the paper is as follows. Section 2 presents the theoretical frame of the study of the charge modulation in a double-$\boldsymbol{k}$ structure. Group theory is then developed in the case of $CeAl_2$ in section 3. Section 4 is devoted to magnetic x-ray scattering, which in our case was mainly used to optimize the experimental conditions. Section 5 describes the study of the charge modulation, and the results are discussed in section 6.

2. Magnetic and magnetostriction free energies for a double-k structure

We summarize here the main results of the expansion of free energy, detailed in the appendix.

In a magnetic structure, the magnetic moments can be expressed as the sum of Fourier components, which, in the case of a double-$\boldsymbol{k}$ structure, can be written:

$$\boldsymbol{m}_j(\boldsymbol{l}) = \boldsymbol{m}_j^{k_1} \mathrm{e}^{-\mathrm{i}\boldsymbol{k_1}\cdot\boldsymbol{l}} + \boldsymbol{m}_j^{k_2} \mathrm{e}^{-\mathrm{i}\boldsymbol{k_2}\cdot\boldsymbol{l}} + \text{c.c.} \tag{1}$$

The second order of the magnetic free energy deduced from equation (A.4) (appendix) is then:

$$U_0 = \sum_{jj'} \sum_{\alpha\beta} \left[J_{jj'\alpha\beta}(\boldsymbol{k_1}) m_{j\alpha}^{k_1} m_{j'\beta}^{-k_1} + J_{jj'\alpha\beta}(\boldsymbol{k_2}) m_{j\alpha}^{k_2} m_{j'\beta}^{-k_2} \right]. \tag{2}$$

Equation (2), underlines that, for a double-$\boldsymbol{k}$ structure, a Fourier component $\boldsymbol{m}^{k_1}$ is associated only with $\boldsymbol{m}^{-k_1}$, and not with the Fourier component $\boldsymbol{m}^{k_2}$ of the equivalent vector $\boldsymbol{k_2}$.

Now considering the displacements induced by the magnetic strains, we extend the expansion of the magnetostrictive free energy for a double-$\boldsymbol{k}$ structure to the fourth order in the magnetic moments $\boldsymbol{m}$ to include the magneto-elastic coupling, following [1]. The leading order terms in the displacement components are second order in $\boldsymbol{m}$ and first order in the displacement vectors $\boldsymbol{u}$:

$$U_1 = U_1^{k_1 k_1} + U_1^{k_2 k_2} + U_1^{k_1 k_2} + U_1^{k_2 k_1}. \tag{3}$$

The expressions of $U_1^{k_i k_i}$ and $U_1^{k_i k_j}$ $(i, j = 1, 2)$, given in the appendix, lead to different types of propagation vectors $\boldsymbol{k}''$ of the strain wave.

(A) For interactions involving magnetic components of the same propagation vector:

$$\boldsymbol{k}'' = \pm 2\boldsymbol{k_1} \text{ (or, equivalently, } \pm 2\boldsymbol{k_2}) \text{ or}$$

$$\boldsymbol{k}'' = 0.$$

$\boldsymbol{k}'' = 0$ will not be considered any further: it corresponds to an overall expansion or compression of the crystal, which is outside the scope of the present paper. For $\boldsymbol{k}'' = \pm 2\boldsymbol{k_1}$, we confirm what has already been stated in the introduction: in the expansion of the free energy, we expect a displacement term which couples with the magnetic moments and corresponds to a propagation vector twice that of the magnetic structure. The contribution to the magnetostrictive free energy $U_1^{k_1 k_1}$, resulting from the coupling of the propagation vector $\boldsymbol{k_1}$ with itself is:

$$U_1^{k_1 k_1} = \sum_{jj'j''} \sum_{\alpha\beta\gamma} B_{jj'j''\alpha\beta\gamma}(\boldsymbol{k_1}) \left\{ m_{j\alpha}^{k_1} m_{j'\beta}^{k_1} u_{j''\gamma}^{-2k_1} + m_{j\alpha}^{-k_1} m_{j'\beta}^{-k_1} u_{j''\gamma}^{2k_1} + m_{j\alpha}^{k_1} m_{j'\beta}^{-k_1} u_{j''\gamma}^{0} \right\}. \tag{4}$$

(B) For interactions involving magnetic components of the different propagation vectors:

$$\boldsymbol{k}'' = \pm(\boldsymbol{k_1} + \boldsymbol{k_2}) \text{ or}$$

$$\boldsymbol{k}'' = \pm(\boldsymbol{k_1} - \boldsymbol{k_2}),$$

which gives for this contribution ($U_1^{k_1 k_2}$, equation (A.16)) to the free energy:

$$U_1^{k_1 k_2} = \sum_{jj'j''} \sum_{\alpha\beta\gamma} C_{jj'j''\alpha\beta\gamma}(\boldsymbol{k_1}, \boldsymbol{k_2}) \times \left\{ m_{j\alpha}^{k_1} m_{j'\beta}^{k_2} u_{j''\gamma}^{-(k_1+k_2)} + m_{j\alpha}^{-k_1} m_{j'\beta}^{-k_2} u_{j''\gamma}^{(k_1+k_2)} + m_{j\alpha}^{k_1} m_{j'\beta}^{-k_2} u_{j''\gamma}^{-(k_1-k_2)} + m_{j\alpha}^{-k_1} m_{j'\beta}^{k_2} u_{j''\gamma}^{(k_1-k_2)} \right\}. \quad (5)$$

The other fourth order terms, which are either purely magnetic, and fourth order in the magnetic components, or related to the strain wave only, and second order in the displacements components, will be neglected, as developed in the appendix.

As a conclusion, in the second order expansion of the magnetic free energy in a multi-$\boldsymbol{k}$ structure, a Fourier component of the magnetic moments can only couple to a another component of the same propagation vector. Now introducing the displacements, the magnetic components of the two different propagation vectors associated in the double-$\boldsymbol{k}$ magnetic structure can couple via a component of displacement in the fourth order term of the free energy. As a consequence, due to the charge modulation associated with the magnetic structure, one can expect charge satellites corresponding to either $\boldsymbol{k_1} + \boldsymbol{k_2}$ or $\boldsymbol{k_1} - \boldsymbol{k_2}$ propagation vectors. This is different from the observation of resonant magnetic scattering at the same positions in multi-$\boldsymbol{k}$ magnetic structures, which is due to second order terms in the resonant magnetic cross section, as pointed out in [9, 10]. The existence of non-resonant $\boldsymbol{k_1} \pm \boldsymbol{k_2}$ satellites may be considered as a new signature of multi-$\boldsymbol{k}$ magnetic structures.

3. Symmetry analysis in the case of $CeAl_2$

Once the values of the propagation vector $\boldsymbol{k}''$ of the lattice modulation are selected, one has to determine the possible components $u_{j''\gamma}^{k''}$ for which the magnetostriction free energy U_1 is invariant in any symmetry operations of the group which leaves $\boldsymbol{k}''$ invariant. This is actually the group which transforms the Fourier components $u_{j''\gamma}^{k''}$ into themselves. This little group $G_{k''}^C$ is constituted of the symmetry elements of the usual little group $G_{k''}$, plus the symmetry elements obtained with the inversion I (h_{25}) associated with the conjugation C operators. Both I and C change $\boldsymbol{k}$ into $-\boldsymbol{k}$, but their product keeps the propagation vector unchanged [16].

The polynomials U_1 can be considered as vectors which span a vectorial space $M \otimes M \otimes U$ with monomials of type $m_{j\alpha}^{k} m_{j'\beta}^{k'} u_{j''\gamma}^{k''}$ for basis vectors. The way the operators h_i of $G_{k''}^C$ transform these basis vectors provides a set of matrices corresponding to a co-representation Λ. Λ is reducible and can be decomposed into irreducible co-representations λ_i, among which λ_1 is the trivial representation with all its characters χ_i equal to 1. The polynomials U_1, which remain invariant under the symmetry operations of $G_{k''}^C$, are those constructed with the basis vectors of the trivial co-representation λ_1 [17]. These basis vectors are obtained with the help of the projection of all the monomials of space $M \otimes M \otimes U$ onto the λ_1 sub-space using the projection operator:

$$P^1 = \sum_i \chi_i^*(\lambda_1) h_i = \sum_i h_i. \quad (6)$$

The Fourier components $m_{j\alpha}^{k}$ and $m_{j'\beta}^{k'}$ involved in the monomials are actually not independent and their relationships, which define the magnetic structure of $CeAl_2$ [14], are summarized in table 1. A simplified form, where the three x, y and z components are considered as equal and where the phase difference φ between them is neglected, is also given in table 1 and will be used here.

Table 1. Relations between the magnetic Fourier components $m_{j\alpha}^{k}$ in the $CeAl_2$ magnetic structure. The exact ones are from [14] and the simplified ones ($|m_x^k| = |m_z^k| = m$ and $\varphi = 0$) are used in this paper.

Exact magnetic structure		Simplified structure	
$m_{1x}^{k_1} = \lvert m_x^k\rvert e^{i\varphi}$	$m_{2x}^{k_1} = -\lvert m_x^k\rvert e^{-i\varphi}$	$m_{1x}^{k_1} = m$	$m_{2x}^{k_1} = -m$
$m_{1y}^{k_1} = \lvert m_x^k\rvert e^{-i\varphi}$	$m_{2y}^{k_1} = -\lvert m_x^k\rvert e^{i\varphi}$	$m_{1y}^{k_1} = m$	$m_{2y}^{k_1} = -m$
$m_{1z}^{k_1} = \lvert m_z^k\rvert$	$m_{2z}^{k_1} = -\lvert m_z^k\rvert$	$m_{1z}^{k_1} = m$	$m_{2z}^{k_1} = -m$
$m_{1x}^{k_2} = i\lvert m_x^k\rvert e^{i\varphi}$	$m_{2x}^{k_2} = i\lvert m_x^k\rvert e^{-i\varphi}$	$m_{1x}^{k_2} = im$	$m_{2x}^{k_2} = im$
$m_{1y}^{k_2} = i\lvert m_x^k\rvert e^{-i\varphi}$	$m_{2y}^{k_2} = i\lvert m_x^k\rvert e^{i\varphi}$	$m_{1y}^{k_2} = im$	$m_{2y}^{k_2} = im$
$m_{1z}^{k_2} = -i\lvert m_z^k\rvert$	$m_{2z}^{k_2} = -i\lvert m_z^k\rvert$	$m_{1z}^{k_2} = -im$	$m_{2z}^{k_2} = -im$

The different types of propagation vectors of the lattice modulation are now considered separately. The following analysis is restricted to one magnetic domain, with propagation vectors $\boldsymbol{k_1} = (1/2 + \delta, 1/2 - \delta, 1/2)$ and $\boldsymbol{k_2} = (1/2 + \delta, 1/2 - \delta, -1/2)$. The transposition to the other domains is straightforward.

3.1. Interactions involving displacement components of the same propagation vector: $\boldsymbol{k}'' = \pm 2\boldsymbol{k_1}$

The little co-group $G_{2k_1}^C$ which leaves $\boldsymbol{k}'' = (2\delta, -2\delta, 0)$ (equivalent to $\boldsymbol{k}'' = (1 + 2\delta, 1 - 2\delta, 1)$ in the first Brillouin zone) unchanged, contains 8 elements h_1, h_{13}, h_{28}, h_{40}, Ch_{25}, Ch_{37}, Ch_4 and Ch_{16} [18], listed in table 2. The projection operator onto the trivial co-representation is:

$$P_{2k_1}^1 = h_1 + h_{13} + h_{28} + h_{40} + Ch_{25} + Ch_{37} + Ch_4 + Ch_{16}. \quad (7)$$

The transformations of the different elements of the $m_{j\alpha}^{k_1} m_{j'\beta}^{k_1} u_{j''\gamma}^{-2k_1}$ monomials are given in table 2. The fractional translations have been omitted in the table, as they cancel out in the final product (factor $e^{(-k_1 - k_1 + 2k_1)}$). Applying $P_{2k_1}^1$ to the different monomials leads to the following three polynomials which are invariant in $G_{2k_1}^C$:

$$U_{2k_1}^1 = m^2 \left[(u_{1z}^{2k_1} + u_{1z}^{*2k_1}) - (u_{2z}^{2k_1} + u_{2z}^{*2k_1}) \right], \quad (8)$$

corresponding to antiparallel displacements of atoms Ce_1 and Ce_2 along [001] in phase with the magnetic modulation.

$$U_{2k_1}^2 = m^2 \left[(u_{1x}^{2k_1} + u_{1x}^{*2k_1}) + (u_{1y}^{2k_1} + u_{1y}^{*2k_1}) - (u_{2x}^{2k_1} + u_{2x}^{*2k_1}) - (u_{2y}^{2k_1} + u_{2y}^{*2k_1}) \right], \quad (9)$$

Table 2. Action of the operators h_i of the little group $G^C_{2\mathbf{k_1}}$ on the Fourier components $m^{-\mathbf{k_1}}_{j\alpha}$ and $u^{2\mathbf{k_1}}_{j''\gamma}$.

h_1 (x, y, z)	h_{13} $(\bar{y}, \bar{x}, \bar{z})$	h_{28} $(x+\frac{1}{4}, y+\frac{3}{4}, \bar{z}+\frac{1}{2})$	h_{40} $(\bar{y}+\frac{1}{4}, \bar{x}+\frac{3}{4}, z+\frac{1}{2})$	Ch_{25} $(\bar{x}, \bar{y}, \bar{z})$	Ch_{37} (y, x, z)	Ch_4 $(\bar{x}+\frac{3}{4}, \bar{y}+\frac{1}{4}, z+\frac{1}{2})$	Ch_{16} $(y+\frac{3}{4}, x+\frac{1}{4}, \bar{z}+\frac{1}{2})$
$m^{-\mathbf{k_1}}_{1x} = m$	$-m^{-\mathbf{k_1}}_{2y} = m$	$-m^{-\mathbf{k_2}}_{2x} = \mathrm{i}m$	$m^{-\mathbf{k_2}}_{1y} = -\mathrm{i}m$	$m^{*-\mathbf{k_1}}_{2x} = -m$	$-m^{*-\mathbf{k_1}}_{1y} = -m$	$-m^{*-\mathbf{k_2}}_{1x} = -\mathrm{i}m$	$m^{*-\mathbf{k_2}}_{2y} = \mathrm{i}m$
$m^{-\mathbf{k_1}}_{1y} = m$	$-m^{-\mathbf{k_1}}_{2x} = m$	$-m^{-\mathbf{k_2}}_{2y} = \mathrm{i}m$	$m^{-\mathbf{k_2}}_{1x} = -\mathrm{i}m$	$m^{*-\mathbf{k_1}}_{2y} = -m$	$-m^{*-\mathbf{k_1}}_{1x} = -m$	$-m^{*-\mathbf{k_2}}_{1y} = -\mathrm{i}m$	$m^{*-\mathbf{k_2}}_{2x} = \mathrm{i}m$
$m^{-\mathbf{k_1}}_{1z} = m$	$-m^{-\mathbf{k_1}}_{2z} = m$	$m^{-\mathbf{k_2}}_{2z} = \mathrm{i}m$	$-m^{-\mathbf{k_2}}_{1z} = -\mathrm{i}m$	$m^{*-\mathbf{k_1}}_{2z} = -m$	$-m^{*-\mathbf{k_1}}_{1z} = -m$	$m^{*-\mathbf{k_2}}_{1z} = -\mathrm{i}m$	$-m^{*-\mathbf{k_2}}_{2z} = \mathrm{i}m$
$m^{-\mathbf{k_1}}_{2x} = -m$	$-m^{-\mathbf{k_1}}_{1y} = -m$	$-m^{-\mathbf{k_2}}_{1x} = \mathrm{i}m$	$m^{-\mathbf{k_2}}_{2y} = -\mathrm{i}m$	$m^{*-\mathbf{k_1}}_{1x} = m$	$-m^{*-\mathbf{k_1}}_{2y} = m$	$-m^{*-\mathbf{k_2}}_{2x} = -\mathrm{i}m$	$m^{*-\mathbf{k_2}}_{1y} = \mathrm{i}m$
$m^{-\mathbf{k_1}}_{2y} = -m$	$-m^{-\mathbf{k_1}}_{1x} = -m$	$-m^{-\mathbf{k_2}}_{1y} = \mathrm{i}m$	$m^{-\mathbf{k_2}}_{2x} = -\mathrm{i}m$	$m^{*-\mathbf{k_1}}_{1y} = m$	$-m^{*-\mathbf{k_1}}_{2x} = m$	$-m^{*-\mathbf{k_2}}_{2y} = -\mathrm{i}m$	$m^{*-\mathbf{k_2}}_{1x} = \mathrm{i}m$
$m^{-\mathbf{k_1}}_{2z} = -m$	$-m^{-\mathbf{k_1}}_{1z} = -m$	$m^{-\mathbf{k_2}}_{1z} = \mathrm{i}m$	$-m^{-\mathbf{k_2}}_{2z} = -\mathrm{i}m$	$m^{*-\mathbf{k_1}}_{1z} = m$	$-m^{*-\mathbf{k_1}}_{2z} = m$	$m^{*-\mathbf{k_2}}_{2z} = -\mathrm{i}m$	$-m^{*-\mathbf{k_2}}_{1z} = \mathrm{i}m$
$u^{2\mathbf{k_1}}_{1x}$	$-u^{2\mathbf{k_1}}_{2y}$	$u^{2\mathbf{k_1}}_{2x}$	$-u^{2\mathbf{k_1}}_{1y}$	$-u^{*2\mathbf{k_1}}_{2x}$	$u^{*2\mathbf{k_1}}_{1y}$	$-u^{*2\mathbf{k_1}}_{1x}$	$u^{*2\mathbf{k_1}}_{2y}$
$u^{2\mathbf{k_1}}_{1y}$	$-u^{2\mathbf{k_1}}_{2x}$	$u^{2\mathbf{k_1}}_{2y}$	$-u^{2\mathbf{k_1}}_{1x}$	$-u^{*2\mathbf{k_1}}_{2y}$	$u^{*2\mathbf{k_1}}_{1x}$	$-u^{*2\mathbf{k_1}}_{1y}$	$u^{*2\mathbf{k_1}}_{2x}$
$u^{2\mathbf{k_1}}_{1z}$	$-u^{2\mathbf{k_1}}_{2z}$	$-u^{2\mathbf{k_1}}_{2z}$	$u^{2\mathbf{k_1}}_{1z}$	$-u^{*2\mathbf{k_1}}_{2z}$	$u^{*2\mathbf{k_1}}_{1z}$	$u^{*2\mathbf{k_1}}_{1z}$	$-u^{*2\mathbf{k_1}}_{2z}$

Table 3. Action of the operators h_i of the little group $G^C_{\mathbf{k_1}+\mathbf{k_2}}$ on the Fourier components $m^{-\mathbf{k_1}}_{j\alpha}$, $m^{-\mathbf{k_2}}_{j\alpha}$ and $u^{\mathbf{k_1}+\mathbf{k_2}}_{j''\gamma}$.

h_1 (x, y, z)	h_{28} $(x+\frac{1}{4}, y+\frac{3}{4}, \bar{z}+\frac{1}{2})$	Ch_{25} $(\bar{x}, \bar{y}, \bar{z})$	Ch_4 $(\bar{x}+\frac{3}{4}, \bar{y}+\frac{1}{4}, z+\frac{1}{2})$
$m^{-\mathbf{k_1}}_{1x} = m$	$-m^{-\mathbf{k_2}}_{2x} = \mathrm{i}m$	$m^{*-\mathbf{k_1}}_{2x} = -m$	$-m^{*-\mathbf{k_2}}_{1x} = -\mathrm{i}m$
$m^{-\mathbf{k_1}}_{1y} = m$	$-m^{-\mathbf{k_2}}_{2y} = \mathrm{i}m$	$m^{*-\mathbf{k_1}}_{2y} = -m$	$-m^{*-\mathbf{k_2}}_{1y} = -\mathrm{i}m$
$m^{-\mathbf{k_1}}_{1z} = m$	$m^{-\mathbf{k_2}}_{2z} = \mathrm{i}m$	$m^{*-\mathbf{k_1}}_{2z} = -m$	$m^{*-\mathbf{k_2}}_{1z} = -\mathrm{i}m$
$m^{-\mathbf{k_1}}_{2x} = -m$	$-m^{-\mathbf{k_2}}_{1x} = \mathrm{i}m$	$m^{*-\mathbf{k_1}}_{1x} = m$	$-m^{*-\mathbf{k_2}}_{2x} = -\mathrm{i}m$
$m^{-\mathbf{k_1}}_{2y} = -m$	$-m^{-\mathbf{k_2}}_{1y} = \mathrm{i}m$	$m^{*-\mathbf{k_1}}_{1y} = m$	$-m^{*-\mathbf{k_2}}_{2y} = -\mathrm{i}m$
$m^{-\mathbf{k_1}}_{2z} = -m$	$m^{-\mathbf{k_2}}_{1z} = \mathrm{i}m$	$m^{*-\mathbf{k_1}}_{1z} = m$	$m^{*-\mathbf{k_2}}_{2z} = -\mathrm{i}m$
$m^{-\mathbf{k_2}}_{1x} = -\mathrm{i}m$	$-m^{-\mathbf{k_1}}_{2x} = m$	$m^{*-\mathbf{k_2}}_{2x} = \mathrm{i}m$	$-m^{*-\mathbf{k_1}}_{1x} = -m$
$m^{-\mathbf{k_2}}_{1y} = -\mathrm{i}m$	$-m^{-\mathbf{k_1}}_{2y} = m$	$m^{*-\mathbf{k_2}}_{2y} = \mathrm{i}m$	$-m^{*-\mathbf{k_1}}_{1y} = -m$
$m^{-\mathbf{k_2}}_{1z} = \mathrm{i}m$	$m^{-\mathbf{k_1}}_{2z} = -m$	$m^{*-\mathbf{k_2}}_{2z} = -\mathrm{i}m$	$m^{*-\mathbf{k_1}}_{1z} = m$
$m^{-\mathbf{k_2}}_{2x} = -\mathrm{i}m$	$-m^{-\mathbf{k_1}}_{1x} = -m$	$m^{*-\mathbf{k_2}}_{1x} = \mathrm{i}m$	$-m^{*-\mathbf{k_1}}_{2x} = m$
$m^{-\mathbf{k_2}}_{2y} = -\mathrm{i}m$	$-m^{-\mathbf{k_1}}_{1y} = -m$	$m^{*-\mathbf{k_2}}_{1y} = \mathrm{i}m$	$-m^{*-\mathbf{k_1}}_{2y} = m$
$m^{-\mathbf{k_2}}_{2z} = \mathrm{i}m$	$m^{-\mathbf{k_1}}_{1z} = m$	$m^{*-\mathbf{k_2}}_{1z} = -\mathrm{i}m$	$m^{*-\mathbf{k_1}}_{2z} = -m$
$u^{(\mathbf{k_1}+\mathbf{k_2})}_{1x}$	$u^{(\mathbf{k_1}+\mathbf{k_2})}_{2x}$	$-u^{*(\mathbf{k_1}+\mathbf{k_2})}_{2x}$	$-u^{*(\mathbf{k_1}+\mathbf{k_2})}_{1x}$
$u^{(\mathbf{k_1}+\mathbf{k_2})}_{1y}$	$u^{(\mathbf{k_1}+\mathbf{k_2})}_{2y}$	$-u^{*(\mathbf{k_1}+\mathbf{k_2})}_{2y}$	$-u^{*(\mathbf{k_1}+\mathbf{k_2})}_{1y}$
$u^{(\mathbf{k_1}+\mathbf{k_2})}_{1z}$	$-u^{(\mathbf{k_1}+\mathbf{k_2})}_{2z}$	$-u^{*(\mathbf{k_1}+\mathbf{k_2})}_{2z}$	$u^{*(\mathbf{k_1}+\mathbf{k_2})}_{1z}$

corresponding to antiparallel displacements of atoms Ce_1 and Ce_2 along [110], in phase with the magnetic modulation, and

$$U^3_{2\mathbf{k_1}} = m^2\big[(u^{2\mathbf{k_1}}_{1x} - u^{*2\mathbf{k_1}}_{1x}) - (u^{2\mathbf{k_1}}_{1y} - u^{*2\mathbf{k_1}}_{1y}) + (u^{2\mathbf{k_1}}_{2x} - u^{*2\mathbf{k_1}}_{2x}) - (u^{2\mathbf{k_1}}_{2y} - u^{*2\mathbf{k_1}}_{2y})\big], \quad (10)$$

corresponding to parallel displacements of atoms Ce_1 and Ce_2 along $[1\bar{1}0]$, in quadrature with the magnetic modulation.

The actual displacements are all the linear combinations of $U^1_{2\mathbf{k_1}}$, $U^2_{2\mathbf{k_1}}$ and $U^3_{2\mathbf{k_1}}$. We note that the direction of the lattice modulation is related only to the incommensurate part $\tau = (\delta, -\delta, 0)$ of the propagation vectors. In the first two cases (8) and (9), the lattice modulation and the magnetic modulation are in phase, and the displacements of both Ce sites are antiparallel, along a direction perpendicular to τ while, in the third case (10), the modulations are in quadrature, and the displacements are parallel, along τ.

*3.2. Interactions involving the sum of the two propagation vectors of the double-**k** structure: $\mathbf{k}'' = \pm(\mathbf{k_1} + \mathbf{k_2})$*

The magnetic little group $G^C_{\mathbf{k_1}+\mathbf{k_2}}$ which leaves $\mathbf{k}'' = (1 + 2\delta, 1 - 2\delta, 0)$ unchanged contains only the 4 symmetry elements h_1, h_{28}, Ch_{25} and Ch_4 [18]. To project all the monomials of the most general expression of $U^{\mathbf{k_1}+\mathbf{k_2}}$ onto the trivial co-representation λ_1, we use the projection operator:

$$P^1_{\mathbf{k_1}+\mathbf{k_2}} = h_1 + h_{28} + Ch_{25} + Ch_4. \quad (11)$$

The transformations of each term of the monomials of type $m^{\mathbf{k_1}}_{j\alpha} m^{\mathbf{k_2}}_{j'\beta} u^{-(\mathbf{k_1}+\mathbf{k_2})}_{j''\gamma}$ are given in table 3. One obtains six polynomials which are invariant in $G^C_{\mathbf{k_1}+\mathbf{k_2}}$:

$$U^1_{\mathbf{k_1}+\mathbf{k_2}} = \mathrm{i}m^2\big[(u^{(\mathbf{k_1}+\mathbf{k_2})}_{1x} + u^{*(\mathbf{k_1}+\mathbf{k_2})}_{1x}) - (u^{(\mathbf{k_1}+\mathbf{k_2})}_{2x} + u^{*(\mathbf{k_1}+\mathbf{k_2})}_{2x})\big], \quad (12)$$

$$U^2_{\mathbf{k_1}+\mathbf{k_2}} = \mathrm{i}m^2\big[(u^{(\mathbf{k_1}+\mathbf{k_2})}_{1x} - u^{*(\mathbf{k_1}+\mathbf{k_2})}_{1x}) + (u^{(\mathbf{k_1}+\mathbf{k_2})}_{2x} - u^{*(\mathbf{k_1}+\mathbf{k_2})}_{2x})\big], \quad (13)$$

$$U^3_{\mathbf{k_1}+\mathbf{k_2}} = \mathrm{i}m^2\big[(u^{(\mathbf{k_1}+\mathbf{k_2})}_{1y} + u^{*(\mathbf{k_1}+\mathbf{k_2})}_{1y}) - (u^{(\mathbf{k_1}+\mathbf{k_2})}_{2y} + u^{*(\mathbf{k_1}+\mathbf{k_2})}_{2y})\big], \quad (14)$$

$$U^4_{\mathbf{k_1}+\mathbf{k_2}} = \mathrm{i}m^2\big[(u^{(\mathbf{k_1}+\mathbf{k_2})}_{1y} - u^{*(\mathbf{k_1}+\mathbf{k_2})}_{1y}) + (u^{(\mathbf{k_1}+\mathbf{k_2})}_{2y} - u^{*(\mathbf{k_1}+\mathbf{k_2})}_{2y})\big], \quad (15)$$

$$U^5_{\mathbf{k_1}+\mathbf{k_2}} = \mathrm{i}m^2\big[(u^{(\mathbf{k_1}+\mathbf{k_2})}_{1z} + u^{*(\mathbf{k_1}+\mathbf{k_2})}_{1z}) - (u^{(\mathbf{k_1}+\mathbf{k_2})}_{2z} + u^{*(\mathbf{k_1}+\mathbf{k_2})}_{2z})\big], \quad (16)$$

$$U^6_{k_1+k_2} = im^2\big[(u^{(k_1+k_2)}_{1z} - u^{*(k_1+k_2)}_{1z}) + (u^{(k_1+k_2)}_{2z} - u^{*(k_1+k_2)}_{2z})\big]. \quad (17)$$

The actual displacements are all the linear combinations of these six polynomials. The displacements are such that the x, y and z components of the same atom are not coupled. The amplitudes are the same for atoms Ce_1 and Ce_2, but with a phase difference.

*3.3. Interactions involving the difference of the two propagation vectors of the double-**k** structure: $\boldsymbol{k''} = \pm(\boldsymbol{k_1} - \boldsymbol{k_2})$*

The little group $G_{k''=(001)}$ which leaves $\boldsymbol{k''} = (0, 0, 1)$ unchanged contains 16 symmetry elements h_1, h_2, h_3, h_4, h_{13}, h_{14}, h_{15}, h_{16}, h_{25}, h_{26}, h_{27}, h_{28}, h_{37}, h_{38}, h_{39}, and h_{40} [18]. As in the previous cases, one has to project all the $m^{-k_1}_{j\alpha} m^{k_2}_{j'\beta} u^{k_1-k_2}_{j''\gamma}$ monomials onto the trivial representation λ_1. However, within this symmetry, neither the little group $G_{k''=(001)}$, nor the magnetic little group $G^C_{k''=(001)}$, have any trivial representation [18]. As a consequence, no displacement $u^{k_1-k_2}_{j''\gamma}$ which keeps monomials of type $m^{-k_1}_{j\alpha} m^{k_2}_{j'\beta} u^{k_1-k_2}_{j''\gamma}$ invariant under all the symmetry operation of the group $G^C_{k''=(001)}$ can exist.

4. X-ray magnetic scattering

Cerium, with only one 4f electron in the magnetic state Ce^{3+} and small magnetic moments is a rather poor candidate for x-ray magnetic scattering studies, and only very few examples are found in the literature [19–22]. The case of $CeAl_2$ is even more delicate due to its reduced moments ($\approx$0.7 μ_B compared to the free ion value of 2.14 μ_B) and to the presence of 6 magnetic k-domains. However, $CeAl_2$ is a typical example of a complex incommensurate magnetic structure and it was felt important to test the above formalism against experimental evidence in this compound.

4.1. Experiments

The experiments were performed at the magnetic scattering beamline ID20 of the ESRF [23], on a single crystalline platelet (about 4 × 6 × 3 mm^3), cleaved perpendicular to a [111] direction. The original ingot was grown using the Bridgman method. The beamline was tuned to different energies below or close to the cerium L_2 and L_3 absorption edges.

The sample was mounted in a liquid helium cryostat, which imposed a horizontal plane scattering geometry. The horizontal incident beam polarization was then parallel to the scattering plane (π polarization). The sample was oriented with its $[11\bar{2}]$ axis vertical, in order to have both the (111) and the $(1\bar{1}0)$ reflections in the horizontal scattering plane, which gives access to the magnetic reflections from a single magnetic domain with a propagation vector $\boldsymbol{k} = (1/2 + \delta, 1/2 - \delta, 1/2)$. Keeping the sample temperature below the Neel temperature (T_N = 3.8 K) turned out to be delicate because of the heat load on the sample: at 5.227 keV, below the cerium L edges, with an incoming flux of 2 × 10^{13} photons s^{-1} at 200 mA, resulting in a power density of about 8–12 mW mm^{-2}, the magnetic intensity vanished within about two minutes of the beam opening, due to sample heating at the surface. The problem was overcome by attenuating the incident beam by a factor 16, hence reducing the photon flux to 1.3×10^{12} photons s^{-1} at 200 mA. Even with these precautions, signals related to the long range magnetic order vanished at a sensor temperature of 2.7 K, indicating a difference of at least 1 K between the temperature of the illuminated sample spot and the temperature measured on the sample holder, at the magnetic phase transition. The measurements were then performed at the lowest reachable cryostat temperature, 1.8 K, with unsaturated moments.

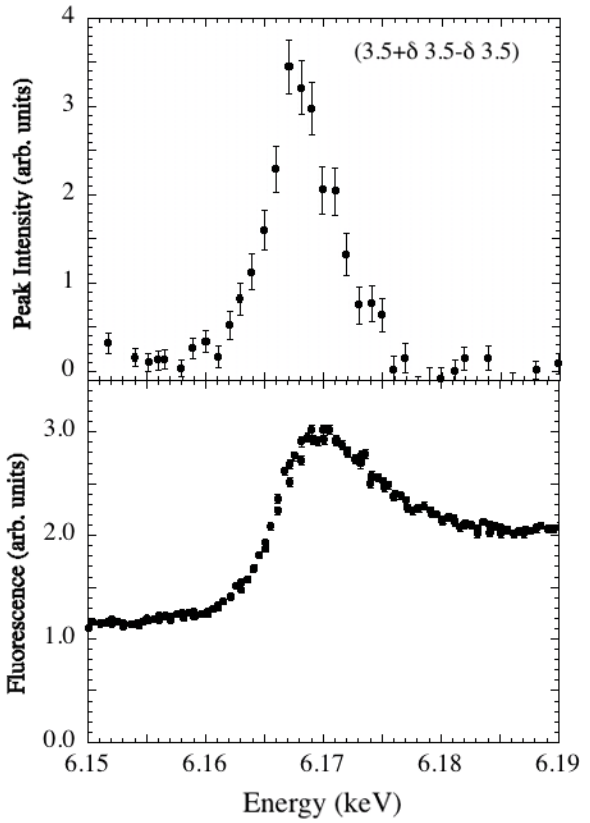

Figure 1. (Top panel) Energy dependence of the $(3.5 + \delta, 3.5 - \delta, 3.5)$ magnetic reflection around the Ce L_2 edge, obtained by scanning the photon energy with a constant scattering vector. The background, measured just away from the peak, has been subtracted. (Bottom panel) Energy dependence of the measured fluorescence.

We first checked the magnetic order by looking for resonant magnetic scattering at the cerium L_2 edge (6.164 keV). We used the (220) reflection of a LiF crystal for polarization analysis, which is very well suited at the L_2 edge, with a Bragg angle of 44.94°. Scanning in the reciprocal space with counting times of 30 seconds/point, we could observe the $(3.5 \pm \delta, 3.5 \mp \delta, 1.5)$, $(2.5 \pm \delta, 2.5 \mp \delta, 2.5)$, and $(1.5 \pm \delta, 1.5 \mp \delta, 1.5)$ magnetic satellites in the rotated π–σ polarization channel, with peak intensities of $\approx$20, 0.5, and 0.07 photons s^{-1}. The observed value of $\delta = 0.112$, is consistent with earlier neutron results. Figure 1 shows the energy dependence

of the peak intensity of the $(3.5 + \delta,\ 3.5 - \delta,\ 3.5)$ reflection, together with the measured fluorescence. The maximum of the resonance is observed at 6.168 keV, close to the energy of the maximum fluorescence. No signal was observed in the unrotated π–π polarization channel.

At the L_3 edge (5.73 keV), using the same analyzer (although it is slightly less convenient here, with a Bragg angle of 49.53°) we observed only an extremely weak magnetic signal (about 1 photon s^{-1}) at the $(3.5 + \delta,\ 3.5 - \delta,\ 3.5)$ position, in the rotated π–σ polarization channel. This signal is observed close to the energy of the maximum absorption and vanishes above and below, like at the L_2 edge.

We also looked for non-resonant magnetic scattering, at an incident photon energy of 5.227 keV, below the cerium L edges, where we could use the (004) reflection from a pyrolytic graphite crystal for polarization analysis. No magnetic signal could be observed, at either the $(1.5 \pm \delta,\ 1.5 \mp \delta,\ 1.5)$ or the $(2.5 \pm \delta,\ 2.5 \mp \delta,\ 2.5)$ positions.

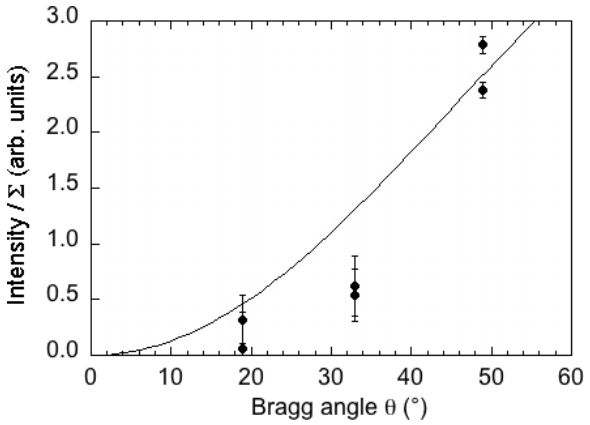

Figure 2. Polarization part of the dipole resonant cross section, $\sin^2\theta$ (line), compared to the measured integrated intensities at the cerium L_2 edge (divided by the structure factor $(\sum e^{iQ\cdot r_j})^2$, for easier comparison).

4.2. Discussion

Resonant x-ray magnetic scattering is interpreted in terms of electric multipole transitions between a core level and a spin (or orbit) polarized empty state above the Fermi level [24]. With incident π polarization and collinear Fourier components of the moments along the scattering vector $\boldsymbol{Q}$ (which is a good approximation for the considered reflections), resonant magnetic scattering is only expected in the π–σ polarization channel with scattering amplitude:

$$F_{\rm res}^{\rm E1} = \frac{4\pi}{|\boldsymbol{k}|} \sum_{\text{site Ce}_j} e^{i\boldsymbol{Q}\cdot\boldsymbol{r}_j} (-i \sin\theta (F_{\rm E1}^{(1)})), \tag{18}$$

$$F_{\rm res}^{\rm E2} = \frac{4\pi}{|\boldsymbol{k}|} \sum_{\text{site Ce}_j} e^{i\boldsymbol{Q}\cdot\boldsymbol{r}_j} \times (-i \sin\theta (F_{\rm E2}^{(1)} \cos^2\theta + F_{\rm E2}^{(3)} \cos 2\theta)), \tag{19}$$

for dipole (E1) and quadrupole (E2) resonances, respectively. θ is the Bragg angle and $\boldsymbol{r}_j$ are the atomic positions. The amplitude factors $F_{\rm EL}^{(n)}$ contain the physics of the resonant process, including the resonant denominator. We note that, in a localized picture of the resonant process, $F_{\rm EL}^{(n)}$ are deduced from atomic calculations [25], which should in our case take into account the modulated character of the magnetic structure. A simple assumption is that the spin and the orbit both follow the same sinusoidal intensity modulation, resulting in a similar modulation of the amplitude factors. For first order terms, this is mathematically equivalent to applying the modulation to the unit vector $\boldsymbol{z}$ in the direction of the moments, as in [26].

Around the cerium $L_{2,3}$ edges, the E1 resonance is expected to dominate the resonant magnetic signal [25]. The fact that, at both edges, the resonance consists in a single peak observed at a photon energy close to the energy of the maximum absorption is consistent with that prediction, as opposed to the multi-peak resonances observed in $Ce(Fe_{1-x}Co_x)_2$, and attributed to either intermediate valence or 4f–3d hybridization effects [22]. The simple dipole origin is further confirmed by the observation of higher intensities at larger $\boldsymbol{Q}$: while the E2 amplitude (equation (19)) has a nonmonotonous angular dependence, the E1 amplitude (equation (18)) increases continuously with θ, consistently with the observation (see next paragraph).

Numerically, the integrated intensities of the measured 6 reflections were corrected for absorption and for Lorentz factor. With incident π polarization, the charge scattering intensities are affected by a factor $\cos^2(2\theta)$. The Lorentz correction for scans in the reciprocal space is $\sin(\theta + \alpha_H)$, where α_H is the angle between the scan direction and the scattering vector [27]. The absorption correction is proportional to $(1 + \sin\alpha/\sin(2\theta - \alpha))$, where α is the angle between the incoming beam and the sample surface. In a first approximation, we neglected the resolution effects from the analyzer crystal, as the x-ray beam from the undulator beamline ID20 is highly collimated. This is a rough approximation in the case of an LiF analyzer crystal with a narrow mosaic spread mosaic (≈0.02°), but acceptable here as long as we consider only orders of magnitude. In figure 2, we compare the factor $\sin^2\theta$ from equation (18) with the integrated intensities divided by the structural term $(\sum e^{i\boldsymbol{Q}\cdot\boldsymbol{r}_j})^2$ ($= \sin^2\pi/8$ or $\cos^2\pi/8$, depending on the reflection). The results are consistent with resonant intensities of dipole origin (E1 resonance), as expected.

In the case of non-resonant scattering, we again make the reasonable approximation that the Fourier components of the moments are close to the [111] direction, i.e. close to the scattering plane. Non-resonant scattering is only expected in the π–σ polarization channel, with a scattering amplitude:

$$F_{\rm non-res}^{\pi-\sigma} = i r_0 \frac{\hbar\omega}{mc^2} \sum_{\text{site Ce}_j} e^{i\boldsymbol{Q}\cdot\boldsymbol{r}_j} (2\sin^2\theta) \times [(L_1 + S_1)\cos\theta - S_3 \sin\theta], \tag{20}$$

where r_0 is the classical electron radius and S and L the Fourier transforms of the spin and orbital magnetic moments. The indices 1 and 3 correspond to the projections along $\boldsymbol{k_i} + \boldsymbol{k_f}$ and $\boldsymbol{k_i} - \boldsymbol{k_f}$ ($=\boldsymbol{Q}$), respectively. For the magnetic reflections $(1.5 \pm \delta,\ 1.5 \mp \delta,\ 1.5)$ and $(2.5 \pm \delta,\ 2.5 \mp \delta,\ 2.5)$, the directions of $\boldsymbol{m}^k$ and $\boldsymbol{Q}$ are both close to the [111] direction, and $L_1 \approx S_1 \approx 0$, $S_3 \approx S_{\rm Ce_j} = S$. The scattering amplitude

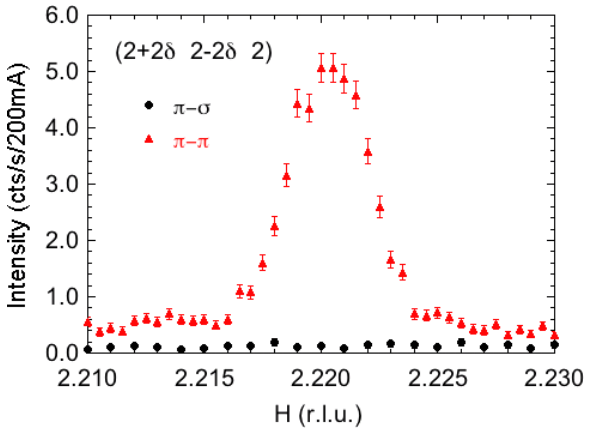

Figure 3. Scans along $[1\bar{1}0]$ at the $(2+2\delta, 2-2\delta, 2)$ charge modulation satellite, in the π–π (triangles) and in the π–σ (circles) polarization channels, measured at a photon energy of 5.227 keV.

simplifies to:

$$F^{\pi-\sigma}_{\text{non-res}} \approx r_0 \frac{\hbar\omega}{mc^2} 4 \sin\frac{\pi}{8} \sin^3\theta\, S. \qquad (21)$$

At 5.227 keV, applying equation (21) and using the free ion value $S = 1/2$ leads to scattering amplitudes $3.5 \times 10^{-4} r_0$ and $1.1 \times 10^{-3} r_0$ for $(1.5 \pm \delta,\ 1.5 \mp \delta,\ 1.5)$ and $(2.5 \pm \delta,\ 2.5 \mp \delta,\ 2.5)$, respectively. For comparison, the calculated charge scattering amplitude of the (111) and (222) reflections are $|F_{(111)}| = 51.4 r_0$ and $|F_{(222)}| = 35.7 r_0$ and the measured scattered intensities in the unrotated π–π polarization channel are about 5200 photons s^{-1} (ph s^{-1}) and 7500 ph s^{-1}, respectively. These measurements required an extra attenuation of the photon beam, by a factor 108 000 at (111) or 5600 at (222). Corrected intensities, including a factor $\cos 2\theta$ for π polarization are of the order of 7×10^8 ph s^{-1} and 2×10^8 ph s^{-1}, respectively. Assuming all 6 magnetic $\boldsymbol{k}$-domains are equally populated then leads to expected non-resonant magnetic intensities in the π–σ polarization channel of the order of 4×10^{-3} ph s^{-1} and 4×10^{-2} ph s^{-1} for $(1.5 \pm \delta,\ 1.5 \mp \delta,\ 1.5)$ and $(2.5 \pm \delta,\ 2.5 \mp \delta,\ 2.5)$, respectively. The $(2.5 \pm \delta,\ 2.5 \mp \delta,\ 2.5)$ reflections could have been observed on top of a measured background of 0.1 ph s^{-1} with long counting times. However, the above calculation does not include the fact the cerium moments are reduced by about a factor 3 as compared to the free ion value, and that they are actually not saturated due to sample heating at the surface (section 4.1). We also note that the calculation involves normalizing intensities over 10 orders of magnitude, which may not be accurate enough.

5. Lattice modulation: x-ray charge scattering

5.1. Experiments

The experiments were performed at the ID20 beamline of the ESRF, first in the same conditions as the magnetic study, section 4.1, then, with a second sample, in a four-circle geometry, rendered possible by the use of a closed-cycle refrigerator, equipped with an additional Joule–Thomson stage (base temperature 1.8 K). In the 2-axis scattering geometry, at a photon energy of 5.227 keV, we could use the (004) reflection of a graphite crystal for polarization analysis: it has a mosaic spread of 0.2°, which is much better suited than LiF to the measurement of integrated intensities. Having only access to a single propagation vector, we concentrated on a study of the satellite reflections corresponding to a propagation vector $2\boldsymbol{k_1}$ (section 5.2). We observed peak intensities of the order of a few counts per second and could measure integrated intensities for a quantitative analysis. In the 4-circle geometry, the beamline was tuned to a slightly higher photon energy, 6.15 keV, just below the cerium L_2 edge, and we used the (220) reflection from a LiF crystal for both polarization analysis and removal of the fluorescence background from the cerium L_3 edge. Even in that more flexible geometry, using a slightly shorter wavelength, we had to tilt the sample inside the cryostat, with the surface normal making an angle of about 57° with the rotation axis of the cryostat. That way, and making full use of the four sample rotations ('azimuthal geometry'), we could access a larger number of non-specular reflections, from all the 6 magnetic domains, listed in table 4. The thermal contact with the sample surface was improved, and we could use a higher photon flux ($\approx 10^{13}$ ph s^{-1}). With this, and improved sample quality, the intensities of the reflections with propagation vector $2\boldsymbol{k_1}$ were then increased by almost two orders of magnitude. We performed a systematic search for charge modulation satellites corresponding to all three possible propagation vectors $2\boldsymbol{k_1}$ (section 5.2), $\boldsymbol{k_1} + \boldsymbol{k_2}$ or $\boldsymbol{k_1} - \boldsymbol{k_2}$ (section 5.3), for a more qualitative study.

Table 4. Magnetic domains of $CeAl_2$, depending on the propagation vectors $\boldsymbol{k_1}$ and $\boldsymbol{k_2}$.

Domains	$\boldsymbol{k_1}$	$\boldsymbol{k_2}$
Domain 1a	$(1/2+\delta, 1/2-\delta, 1/2)$	$(1/2+\delta, 1/2-\delta, -1/2)$
Domain 1b	$(1/2+\delta, -1/2+\delta, 1/2)$	$(1/2+\delta, -1/2+\delta, -1/2)$
Domain 2a	$(1/2, 1/2+\delta, 1/2-\delta)$	$(-1/2, 1/2+\delta, 1/2-\delta)$
Domain 2b	$(1/2, 1/2+\delta, -1/2+\delta)$	$(-1/2, 1/2+\delta, -1/2+\delta)$
Domain 3a	$(1/2+\delta, 1/2, 1/2-\delta)$	$(1/2+\delta, -1/2, 1/2-\delta)$
Domain 3b	$(1/2+\delta, 1/2, -1/2+\delta)$	$(1/2+\delta, -1/2, -1/2+\delta)$

5.2. Propagation vector $2\boldsymbol{k}$

5.2.1. Results. In the 2-axis geometry, scans in reciprocal space were measured along the $[1\bar{1}0]$ direction, at positions $(h \pm 2\delta,\ h \mp 2\delta,\ h)$, with $h = 1$–3. In the π–π polarization channel, the scattered intensity was observed at all the investigated satellites, whereas none was detected in the π–σ configuration (figure 3). These intensities vanish above T_N, which proves the connection to the long range magnetic order (figure 4). The energy dependence of the $(2+2\delta,\ 2-2\delta,\ 2)$ modulation satellite around the cerium L_2 edge is shown in figure 5. Although the statistics is rather poor, we note that the energy dependence of this modulation satellite is (slightly but undoubtedly) different from that of the (222) charge Bragg peak, also shown in figure 5. Only the aluminum atoms contribute to the (222) structure factor and the energy dependence reflects only the variation of the linear absorption coefficient. A different behavior, attributed

Table 5. Integrated intensities of charge modulation satellites, measured at 5.227 keV. Intensities have been normalized to the monitor count rate, and are given in ph Å^{-1}/monitor. The correction in the case of the structural peaks (111) and (222) includes the extra attenuation (see the text). The values of $|\boldsymbol{u}|/a$ if $\boldsymbol{u}\|[110]$ are equal to those for $\boldsymbol{u}\|[001]$ divided by $\sqrt{2}$.

$\boldsymbol{Q}$	Imeas	Icor	$F_{\rm calc}/r_0$	$\boldsymbol{Q}\cdot\boldsymbol{u}$	$\|\boldsymbol{u}\|/a$ for $\boldsymbol{u}\|[001]$
(111)	2.2 (2) $\times 10^3$	8.7 (9) $\times 10^7$	51.4		
(222)	2.93 (2) $\times 10^2$	9.0 (9) $\times 10^7$	35.7		
$(1+2\delta, 1-2\delta, 1)$	1.50 (7)	2.15 (10)	36.7 $\boldsymbol{Q}\cdot\boldsymbol{u}$	4.4 (1) $\times 10^{-5}$	6.9 (2) $\times 10^{-6}$
$(1-2\delta, 1+2\delta, 1)$	0.46 (5)	3.8 (4)	36.7 $\boldsymbol{Q}\cdot\boldsymbol{u}$	5.8 (3) $\times 10^{-5}$	9.3 (5) $\times 10^{-6}$
$(2+2\delta, 2-2\delta, 2)$	2.3 (3)	15 (2)	45.3 $\boldsymbol{Q}\cdot\boldsymbol{u}$	11.0 (6) $\times 10^{-5}$	8.8 (5) $\times 10^{-6}$
$(2-2\delta, 2+2\delta, 2)$	0.97 (4)	9.2 (4)	45.3 $\boldsymbol{Q}\cdot\boldsymbol{u}$	8.8 (2) $\times 10^{-5}$	7.0 (2) $\times 10^{-6}$
$(3+2\delta, 3-2\delta, 3)$	0.106 (13)	3.8 (4)	25.5 $\boldsymbol{Q}\cdot\boldsymbol{u}$	10.0 (6) $\times 10^{-5}$	5.3 (3) $\times 10^{-6}$

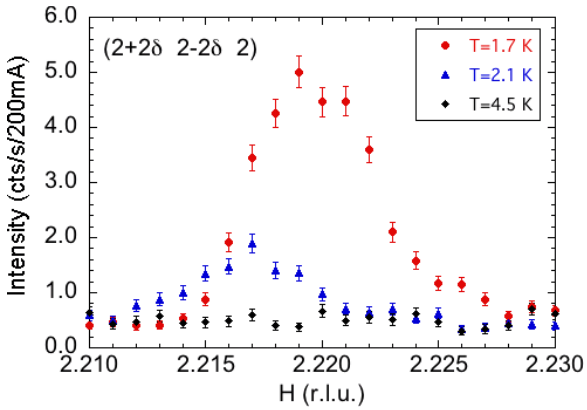

Figure 4. Scans along $[1\bar{1}0]$ at the $(2+2\delta, 2-2\delta, 2)$ charge modulation satellite at different temperatures, measured in the π–π polarization channel, at a photon energy of 5.227 keV.

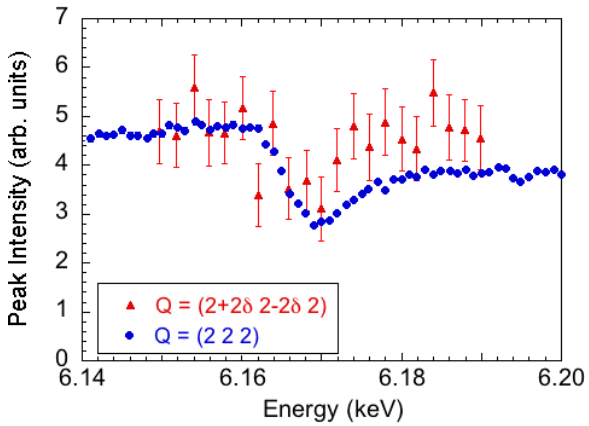

Figure 5. Energy dependence of the $(2+2\delta, 2-2\delta, 2)$ charge modulation satellite and the (222) charge Bragg peak around the Ce L_2 edge. The background, measured just away from the peak, has been subtracted. The intensities have been scaled to coincide below the edge and allow easier comparison.

to diffraction absorption fine structure (DAFS) is generally observed at the absorption edge of an element which does contribute to the structure factor of the studied reflection. The observed energy dependence of the reflection is then consistent with our assumption that it comes mainly from a charge modulation related the Ce atoms, induced by the magnetic modulation.

Table 5 summarizes the integrated intensities of the observed charge modulation satellites, as well as those of the (111) and (222) structural Bragg peaks, measured for scaling, with some additional attenuation of the photon beam by a factor 108 000 and 5 600, respectively. All intensities were corrected for Lorentz factor and absorption, as described in section 4.2. The calculated structure factors are also listed in the table. We note a small discrepancy between the scale factors obtained from either reflection: $K = 2.3 \times 10^4$ and 1.6×10^4 at (111) and (222), respectively. This cannot be related to extinction effects, as the stronger (111) reflection would be more affected. However, the attenuations used at either reflections differ by a factor ≈20, which may induce errors in the normalization. On top of that, both reflections are actually sampling regions of the crystal of different extensions, and we can consider the agreement as reasonable here. To reduce the latter effect on our analysis, we scale the charge modulation intensities using the intensity of the structural Bragg peak closest in the reciprocal space.

Table 6 gives the peak intensities measured in the 4-circle geometry. Reflections are observed for all magnetic domains and they are systematically stronger for domain 1a, showing that, in the second sample, all domains were populated, although not equally. A more accurate determination on the domain populations would be difficult, as each reflection is sampling a different part of the crystal, with possibly different domain populations. This would constitute a different study, but would not affect the main conclusions of the present paper.

5.2.2. Discussion. The intensities representative of the charge modulation satellites are directly related to the amplitude of the modulation [28, 29]. Symmetry considerations have shown that the displacements of sites Ce_1 and Ce_2 have components either parallel or antiparallel. We can write the atomic positions as:

$$\boldsymbol{r}_{lj} = \boldsymbol{L}_l + \boldsymbol{r}_j^{\rm o} + \epsilon_j \boldsymbol{u}_j \sin(2\boldsymbol{k}\cdot\boldsymbol{L}_l), \qquad (22)$$

with $j = 1$ or 2. $\boldsymbol{L}_l$ is a lattice vector, $\boldsymbol{r}_j^{\rm o}$ is the equilibrium position of site j, and $\boldsymbol{u}_j$ is the vector amplitude of the modulation of wave vector $2\boldsymbol{k} = (2\delta, -2\delta, 0)$. We use $\epsilon_1 = 1$ and $\epsilon_2 = 1$ or -1 for displacements parallel or antiparallel to Ce_1, respectively. The scattering amplitude at position $\boldsymbol{Q}$ in the reciprocal space is given by the Fourier transform of the atomic density:

$$F_{\rm mod}(\boldsymbol{Q}) = r_0 f_{\rm Ce} \sum_{l,j} {\rm e}^{{\rm i}\boldsymbol{Q}\cdot\boldsymbol{r}_{lj}}, \qquad (23)$$

Table 6. Peak intensities observed for displacement reflections with $\boldsymbol{k}'' = 2\boldsymbol{k_1}$.

Domain	h	k	l	$(HKL) \pm \boldsymbol{k}''$	N (cts s^{-1})
$2\boldsymbol{k_1} = (2\delta, -2\delta, 0)$	$5+2\delta$	$1-2\delta$	1	$(511)^+$	130 (5)
Domain 1a	$5-2\delta$	$1+2\delta$	1	$(511)^-$	90 (6)
	$6+2\delta$	$2-2\delta$	-2	$(62\bar{2})^+$	134 (3)
$2\boldsymbol{k_1} = (2\delta, 2\delta, 0)$	$5-2\delta$	$1-2\delta$	1	$(511)^-$	1.3 (3)
Domain 1b	$6+2\delta$	2δ	-2	$(60\bar{2})^+$	<0.4
	$6-2\delta$	$2-2\delta$	-2	$(62\bar{2})^-$	8.5 (6)
$2\boldsymbol{k_1} = (0, 2\delta, -2\delta)$	4	2δ	-2δ	$(400)^+$	<0.1
Domain 2a	5	$1+2\delta$	$1-2\delta$	$(511)^+$	8.5 (7)
	5	$1-2\delta$	$1+2\delta$	$(511)^-$	1.1 (5)
	6	2δ	$-2-2\delta$	$(60\bar{2})^+$	<0.4
$2\boldsymbol{k_1} = (0, 2\delta, 2\delta)$	4	2δ	2δ	$(400)^+$	<0.1
Domain 2b	6	$2+2\delta$	$-2+2\delta$	$(62\bar{2})^+$	21 (1)
$2\boldsymbol{k_1} = (2\delta, 0, -2\delta)$	$4+2\delta$	0	-2δ	$(400)^+$	<0.2
Domain 3a	$5+2\delta$	1	$1-2\delta$	$(511)^+$	14 (1)
	$6+2\delta$	0	$-2-2\delta$	$(60\bar{2})^+$	<0.3
	$6+2\delta$	2	$-2-2\delta$	$(62\bar{2})^+$	16 (1)
$2\boldsymbol{k_1} = (2\delta, 0, 2\delta)$	$6-2\delta$	0	$-2-2\delta$	$(60\bar{2})^-$	<0.3
Domain 3b					

where f_{Ce} is the atomic form factor. Using the Jacobi–Anger transformation, which uses the Bessel functions J_n,

$$\mathrm{e}^{\mathrm{i}z\sin\phi} = \sum_{n=-\infty}^{+\infty} \mathrm{e}^{\mathrm{i}n\phi} J_n(z), \tag{24}$$

this transforms into:

$$F_{\mathrm{mod}}(\boldsymbol{Q}) = r_0 f_{\mathrm{Ce}} \sum_{n=-\infty}^{+\infty} \sum_{l} \mathrm{e}^{\mathrm{i}(\boldsymbol{Q}+n2\boldsymbol{k})\cdot\boldsymbol{L}_l} \times \sum_{\mathrm{Ce}_1,\mathrm{Ce}_2} J_n(\boldsymbol{Q}\cdot\boldsymbol{u}_j)\mathrm{e}^{\mathrm{i}\boldsymbol{Q}\cdot\boldsymbol{r}_j^0}, \tag{25}$$

which is finite for $\boldsymbol{Q} + n2\boldsymbol{k}$ a vector of the reciprocal lattice. For small displacements, we can expand equation (23) using the asymptotic form of the Bessel functions. The order $n = 0$ is the usual Thomson scattering. The first order corresponds to satellites at positions $\boldsymbol{G} \pm 2\boldsymbol{k}$ ($\boldsymbol{G}$ being a node of the reciprocal lattice), with structure factor

$$F_{\mathrm{mod}}(\boldsymbol{Q}) = r_0 f_{\mathrm{Ce}} \sum_{\mathrm{Ce}_1,\mathrm{Ce}_2} \left[\frac{\boldsymbol{Q}\cdot\boldsymbol{u}_j}{2}\mathrm{e}^{\mathrm{i}\boldsymbol{Q}\cdot\boldsymbol{r}_j^0}\right]. \tag{26}$$

Summing over the two cerium sites of $CeAl_2$ in domain 1a ($2\boldsymbol{k} = (2\delta, -2\delta, 0)$) leads to, at $\boldsymbol{Q} = (hkl)$:

$$F_{\mathrm{mod}}(\boldsymbol{Q}) = r_0 f_{\mathrm{Ce}}(\boldsymbol{Q}\cdot\boldsymbol{u})\cos[(h+k+l)\pi/4], \tag{27}$$

or

$$F_{\mathrm{mod}}(\boldsymbol{Q}) = \mathrm{i}r_0 f_{\mathrm{Ce}}(\boldsymbol{Q}\cdot\boldsymbol{u})\sin[(h+k+l)\pi/4], \tag{28}$$

for parallel or antiparallel Ce_1 and Ce_2 displacements, respectively. This result is valid in any of the 6 magnetic domains, using the proper permutations of indices in the symmetry analysis.

We note that, in table 6, none of the satellites of the (400) and (60$\bar{2}$) reflections was detected, which tends to show that the strain wave involves only antiparallel displacements of sites Ce_1 and Ce_2 (equation (28)). This is consistent with the observation of scattered intensity at $\boldsymbol{Q} = (2 \pm 2\delta, 2 \mp 2\delta, 2)$, which is allowed by equation (28) but for which equation (27) gives zero intensity.

The structure factors are calculated using equation (28), and listed as F_{calc} in table 5. The calculation empirically assumes all 6 domains equally populated. The amplitude of the modulation is $|\boldsymbol{u}| = (\boldsymbol{Q}\cdot\boldsymbol{u}/\beta) \times a$, where a is the lattice constant and β a geometrical factor, the value of which depends on the direction of the modulation. In domain 1a, $\beta = 2\pi(h+k)/\sqrt{2}$ or $\beta = 2\pi l$ for a modulation along (110) or (001), respectively.

The resulting amplitude $|\boldsymbol{u}|$ of the displacements is of the order of 5–9 $\times$ 10^{-6} lattice units. We may note that, as we expect the order parameter of the charge modulation to follow that of the magnetic structure, the amplitude of the modulation may not be maximum in our experimental conditions, but the order of magnitude should be right. The intensities of the charge modulation satellites are seven orders of magnitude smaller than those of the structural Bragg peaks, hence the need for the dynamical range of a high intensity x-ray beam.

5.3. *Propagation vector* $\boldsymbol{k_1} \pm \boldsymbol{k_2}$

In the four-circle scattering geometry, we searched systematically for satellites from all 6 magnetic domains with propagation vectors $\boldsymbol{k}'' = \pm(\boldsymbol{k_1} + \boldsymbol{k_2})$ and $\pm(\boldsymbol{k_1} - \boldsymbol{k_2})$. For $\boldsymbol{k}'' = \pm(\boldsymbol{k_1} + \boldsymbol{k_2})$, we measured peak intensities, after adjusting the diffractometer angles to maximize the intensity and subtracted the background measured away from the peak (table 7). For $\boldsymbol{k}'' = \pm(\boldsymbol{k_1} - \boldsymbol{k_2})$, the propagation vector is of type (001) (or (100) or (010)), and the possible reflections are at the nodes of the simple cubic lattice, which are forbidden in the faced centered cubic space group. These reflections were centered using the harmonic wavelength $\lambda/2$, not completely filtered out. In that case, the peak intensities, given in table 8

Table 7. Peak intensities observed for displacement reflections with $\boldsymbol{k}'' = \boldsymbol{k_1} + \boldsymbol{k_2}$.

Domains	h	k	l	$(HKL) \pm \boldsymbol{k}''$	N (cts s^{-1})
$\boldsymbol{k_1} + \boldsymbol{k_2} = (1+2\delta, 1-2\delta, 0)$	$5+2\delta$	$1-2\delta$	0	$(400)^+$	2.5 (2)
Domain 1a	$5-2\delta$	$1+2\delta$	0	$(620)^-$	0.92 (20)
$\boldsymbol{k_1} + \boldsymbol{k_2} = (1+2\delta, 1+2\delta, 0)$	$4+2\delta$	2δ	1	$(3\bar{1}1)^+$	0.17 (10)
Domain 1b	$5+2\delta$	$1+2\delta$	0	$(400)^+$	<0.10
$\boldsymbol{k_1} + \boldsymbol{k_2} = (0, 1+2\delta, 1-2\delta)$	4	$1+2\delta$	$1-2\delta$	$(400)^+$	0.17 (10)
Domain 2a	5	2δ	$-2-2\delta$	$(5\bar{1}\bar{3})^+$	2.5 (2)
	5	2δ	-2δ	$(5\bar{1}\bar{1})^+$	8.8 (3)
	5	-2δ	2δ	$(511)^-$	10.3 (4)
$\boldsymbol{k_1} + \boldsymbol{k_2} = (0, 1+2\delta, 1+2\delta)$	4	$1+2\delta$	$1+2\delta$	$(400)^+$	3.8 (3)
Domain 2b	5	2δ	$-2+2\delta$	$(5\bar{1}\bar{3})^+$	1.3 (2)
	5	2δ	2δ	$(5\bar{1}\bar{1})^+$	5.0 (3)
	5	-2δ	-2δ	$(511)^-$	3.9 (3)
	6	$1+2\delta$	$-1+2\delta$	$(60\bar{2})^+$	13.3 (5)
$\boldsymbol{k_1} + \boldsymbol{k_2} = (1+2\delta, 0, 1-2\delta)$	$4+2\delta$	1	-2δ	$(31\bar{1})^+$	1.5 (2)
Domain 3a	$5+2\delta$	0	$1-2\delta$	$(400)^+$	0.17 (10)
$\boldsymbol{k_1} + \boldsymbol{k_2} = (1+2\delta, 0, 1+2\delta)$ Domain 3b	$4+2\delta$	1	2δ	$(31\bar{1})^+$	0.33 (10)

Table 8. Peak intensities observed for displacement reflections with $\boldsymbol{k}'' = \boldsymbol{k_1} - \boldsymbol{k_2}$.

Domains	h	k	l	$(HKL) \pm \boldsymbol{k}''$	N (cts s^{-1})
$\boldsymbol{k_1} - \boldsymbol{k_2} = (001)$	6	2	$\bar{1}$	$(62\bar{2})^+$ or $(620)^-$	<0.05
Domains 1a and 1b	5	1	0	$(51\bar{1})^+$ or $(511)^-$	<0.05
$\boldsymbol{k_1} - \boldsymbol{k_2} = (100)$	4	1	1	$(311)^+$ or $(511)^-$	< 0.05
Domains 2a and 2b	5	0	0	$(400)^+$ or $(600)^-$	<0.05
	5	0	$\bar{2}$	$(40\bar{2})^+$ or $(60\bar{2})^-$	<0.05
	6	1	$\bar{1}$	$(51\bar{1})^+$ or $(71\bar{1})^-$	<0.05
$\boldsymbol{k_1} - \boldsymbol{k_2} = (010)$	5	0	1	$(5\bar{1}1)^+$ or $(511)^-$	4.1(3)
Domains 3a and 3b	4	1	0	$(400)^+$ or $(420)^-$	<0.05

are obtained by subtracting the background measured above T_N.

Table 7 shows that reflections corresponding to a propagation vector $\boldsymbol{k_1} + \boldsymbol{k_2}$ do exist, as expected. Intensities were observed for all magnetic domains, with intensities in most cases smaller than those observed for reflections corresponding to a propagation vector $2\boldsymbol{k_1}$.

Table 8 shows that the reflections corresponding to the propagation vector $(\boldsymbol{k_1} - \boldsymbol{k_2})$ do not exist, with the exception of reflection (501). We note that this reflection, indexed as either $(5\bar{1}1)^+$ or $(511)^-$, is found only in domains 3a and 3b. The equivalent reflections in the other 4 domains were not detected. This is typical of multiple scattering effects, to which we attribute the observation of the (501) reflection. This anomaly set apart, table 8 confirms the predictions of group theory: there are no reflections for a propagation vector of type $(\boldsymbol{k_1} - \boldsymbol{k_2})$.

6. Conclusion

Group theory is a recognized tool in the determination of magnetic structures. We have extended its use to the study of the associated strain wave. In the general case, it allows one to predict the directions of the displacements. In multi-$\boldsymbol{k}$ magnetic structures, strain waves with 'simple' $2\boldsymbol{k}$ or 'combined' $\boldsymbol{k_1} \pm \boldsymbol{k_2}$ propagation vectors are predicted. In the particular case of $CeAl_2$, symmetry analysis has shown that reflections corresponding to propagation vectors $\boldsymbol{k_1} + \boldsymbol{k_2}$ are actually expected, while propagation vectors $\boldsymbol{k_1} - \boldsymbol{k_2}$ are forbidden. Only the use of symmetry arguments could explain this absence of one type of combined propagation vectors.

More generally, differentiating a multi-$\boldsymbol{k}$ magnetic structure from a single-$\boldsymbol{k}$, multi-domain magnetic structure is often a challenge. Using magnetic neutron scattering for example, one must apply an external perturbation to try and unbalance the potential domain populations. However, failure to observe an effect may not be conclusive, and the external perturbation may also modify the intrinsic magnetic configuration. One can also use resonant x-ray magnetic scattering and look for reflections with a $\boldsymbol{k_1} \pm \boldsymbol{k_2}$ propagation vector, allowed by the second order term in the resonant cross section. This may prove experimentally difficult, as the intensity of the $\boldsymbol{k_1} \pm \boldsymbol{k_2}$ peaks is about two orders of magnitude smaller than the simple $\boldsymbol{k_1}$ or $\boldsymbol{k_2}$ peaks [10]. Such peaks are easily observed at the $M_{4,5}$ edges of actinides, where the resonance is huge. Observation will certainly be more difficult for weaker resonances, like the $L_{2,3}$ edges of rare earths, or K edges of transition elements.

We have demonstrated that an original method consists in taking advantage of the strain waves associated with the magnetic structure. Only multi-$\boldsymbol{k}$ structures may lead to a strain wave with a $\boldsymbol{k_1} \pm \boldsymbol{k_2}$ propagation vector. In the case of $CeAl_2$, where the amplitude of the strain wave is less than 10^{-5} lattice units, the observed intensities are of the same order as the resonant magnetic intensities, whether for $2\boldsymbol{k}$ or $\boldsymbol{k_1} + \boldsymbol{k_2}$ propagation vectors, hence stronger than expected for second order resonant magnetic intensities. This method also has the advantage of not being restricted to particular elements and absorption edges.

Appendix. Free energy calculation

We investigate the coupling of the magnetic moments to periodic lattice modulations. The most simple free energy expansion than can describe such a system is fourth order in the magnetic moments, including terms of second and fourth order in the magnetic moments $\boldsymbol{m}$ and first and second order in the periodic displacement vector $\boldsymbol{u}$ [1]. The positive coefficients of the $\boldsymbol{m}^4$ and $\boldsymbol{u}^2$ terms ensure the stability of the system. The $\boldsymbol{m}^4$ terms have been shown to be responsible for the double-$\boldsymbol{k}$ character of the magnetic structure [15]. Upon crossing the phase transition, the coefficient of the $\boldsymbol{m}^2$ term becomes negative, leading to a minimum in the free energy at finite $\boldsymbol{m}$.

The second order term in the expansion of the magnetic free energy of a crystal in the paramagnetic state can be written:

$$U_0 = \sum_{ll'} \sum_{jj'} \sum_{\alpha\beta} J_{ll'jj'\alpha\beta} m_{j\alpha}(\boldsymbol{l}) m_{j'\beta}(\boldsymbol{l}') \tag{A.1}$$

where the $m_{j\alpha}(\boldsymbol{l})$ represent the components of the magnetic moments $m_j(\boldsymbol{l})$, $\boldsymbol{l}$ and $\boldsymbol{l}'$ labeling the crystal cell, j and j' the magnetic atom in the cell, and α and β the axes x, y or z. $J_{ll'jj'\alpha\beta}$ are the exchange interactions between these components of the magnetic atoms.

Introducing the Fourier expansion:

$$\boldsymbol{m}_j(\boldsymbol{l}) = \sum_{\boldsymbol{k}} \boldsymbol{m}_j^{\boldsymbol{k}} \mathrm{e}^{-\mathrm{i}\boldsymbol{k}\cdot\boldsymbol{l}} \tag{A.2}$$

and the Fourier transform of $J_{ll'jj'\alpha\beta}$:

$$J_{jj'\alpha\beta}(\boldsymbol{k}) = \sum_{l} J_{ll'jj'\alpha\beta} \mathrm{e}^{-\mathrm{i}\boldsymbol{k}\cdot(l-l')} \tag{A.3}$$

the second order term of the magnetic free energy U_0 becomes

$$U_0 = \sum_{jj'} \sum_{\alpha\beta} \sum_{\boldsymbol{k}} J_{jj'\alpha\beta}(\boldsymbol{k}) m_{j\alpha}^{\boldsymbol{k}} m_{j'\beta}^{-\boldsymbol{k}}. \tag{A.4}$$

Now looking for the possible displacements due to the magnetic ordering below T_N, we investigate the coupling of the known magnetic structure to the elastic modulations. As such, the magnetic order parameter may be treated as a constant in the free energy, and only the elastic modulations as free variables to be minimized. The first terms of the free energy which couples the magnetic structure and the displacements of the magnetic atom are linear in $\boldsymbol{u}$ and quadratic in $\boldsymbol{m}$:

$$U_1 = \sum_{ll'l''} \sum_{jj'j''} \sum_{\alpha\beta\gamma} A_{ll'l''jj'j''\alpha\beta\gamma} m_{j\alpha}(\boldsymbol{l}) m_{j'\beta}(\boldsymbol{l}') u_{j''\gamma}(\boldsymbol{l}'') \tag{A.5}$$

where $u_{j\alpha}(\boldsymbol{l})$ represent the components of the displacements.

Similarly to what has been done for the moments (equation (A.2)), the displacements can be written as a Fourier expansion (sum over all possible $\boldsymbol{k}''$):

$$\boldsymbol{u}_j(\boldsymbol{l}) = \sum_{\boldsymbol{k}''} \boldsymbol{u}_j^{\boldsymbol{k}''} \mathrm{e}^{-\mathrm{i}\boldsymbol{k}''\cdot\boldsymbol{l}}. \tag{A.6}$$

Once the double-$\boldsymbol{k}$ magnetic structure is set up, the propagation vectors $\boldsymbol{k_1}$ and $\boldsymbol{k_2}$ are well defined, and the magnetic moment components are given by:

$$m_{j\alpha}(\boldsymbol{l}) = \boldsymbol{m}_{j\alpha}^{\boldsymbol{k_1}} \mathrm{e}^{-\mathrm{i}\boldsymbol{k_1}\cdot\boldsymbol{l}} + \boldsymbol{m}_{j\alpha}^{\boldsymbol{k_2}} \mathrm{e}^{-\mathrm{i}\boldsymbol{k_2}\cdot\boldsymbol{l}} + \text{c.c.} \tag{A.7}$$

The magnetostrictive free energy is composed of four terms:

$$U_1 = U_1^{\boldsymbol{k_1}\boldsymbol{k_1}} + U_1^{\boldsymbol{k_2}\boldsymbol{k_2}} + U_1^{\boldsymbol{k_1}\boldsymbol{k_2}} + U_1^{\boldsymbol{k_2}\boldsymbol{k_1}}. \tag{A.8}$$

The first two terms involve interactions between magnetic components of the same propagation vector:

$$\begin{aligned} U_1^{\boldsymbol{k_1}\boldsymbol{k_1}} = & \sum_{ll'l''} \sum_{\boldsymbol{k}''} \sum_{jj'j''} \sum_{\alpha\beta\gamma} A_{ll'l''jj'j''\alpha\beta\gamma} \\ & \times (m_{j\alpha}^{\boldsymbol{k_1}} \mathrm{e}^{-\mathrm{i}\boldsymbol{k_1}\cdot\boldsymbol{l}} + m_{j\alpha}^{-\boldsymbol{k_1}} \mathrm{e}^{\mathrm{i}\boldsymbol{k_1}\cdot\boldsymbol{l}}) \\ & \times (m_{j'\beta}^{\boldsymbol{k_1}} \mathrm{e}^{-\mathrm{i}\boldsymbol{k_1}\cdot\boldsymbol{l}'} + m_{j'\beta}^{-\boldsymbol{k_1}} \mathrm{e}^{\mathrm{i}\boldsymbol{k_1}\cdot\boldsymbol{l}'}) u_{j''\gamma}^{\boldsymbol{k}''} \mathrm{e}^{-\mathrm{i}\boldsymbol{k}''\cdot\boldsymbol{l}''}. \end{aligned} \tag{A.9}$$

In the last two terms, the interactions between magnetic components correspond to different propagation vectors:

$$\begin{aligned} U_1^{\boldsymbol{k_1}\boldsymbol{k_2}} = & \sum_{ll'l''} \sum_{\boldsymbol{k}''} \sum_{jj'j''} \sum_{\alpha\beta\gamma} A_{ll'l''jj'j''\alpha\beta\gamma} \\ & \times (m_{j\alpha}^{\boldsymbol{k_1}} \mathrm{e}^{-\mathrm{i}\boldsymbol{k_1}\cdot\boldsymbol{l}} + m_{j\alpha}^{-\boldsymbol{k_1}} \mathrm{e}^{\mathrm{i}\boldsymbol{k_1}\cdot\boldsymbol{l}}) \\ & \times (m_{j'\beta}^{\boldsymbol{k_2}} \mathrm{e}^{-\mathrm{i}\boldsymbol{k_2}\cdot\boldsymbol{l}'} + m_{j'\beta}^{-\boldsymbol{k_2}} \mathrm{e}^{\mathrm{i}\boldsymbol{k_2}\cdot\boldsymbol{l}'}) u_{j''\gamma}^{\boldsymbol{k}''} \mathrm{e}^{-\mathrm{i}\boldsymbol{k}''\cdot\boldsymbol{l}''}. \end{aligned} \tag{A.10}$$

Both expressions $U_1^{\boldsymbol{k_1}\boldsymbol{k_1}}$ and $U_1^{\boldsymbol{k_1}\boldsymbol{k_2}}$ are themselves the sum of four terms.

In expression $U_1^{\boldsymbol{k_1}\boldsymbol{k_1}}$, if we introduce $\mathrm{e}^{2\mathrm{i}\boldsymbol{k_1}\cdot\boldsymbol{l}''} \mathrm{e}^{-2\mathrm{i}\boldsymbol{k_1}\cdot\boldsymbol{l}''} = 1$ in the first two terms and $\mathrm{e}^{\mathrm{i}\boldsymbol{k_1}\cdot\boldsymbol{l}''} \mathrm{e}^{-\mathrm{i}\boldsymbol{k_1}\cdot\boldsymbol{l}''} = 1$ in the last two terms, we obtain, for instance for the first of the four terms:

$$\begin{aligned} & \sum_{\boldsymbol{k}''} \sum_{jj'j''} \sum_{\alpha\beta\gamma} m_{j\alpha}^{\boldsymbol{k_1}} m_{j'\beta}^{\boldsymbol{k_1}} u_{j''\gamma}^{\boldsymbol{k}''} \sum_{l''} \mathrm{e}^{-\mathrm{i}(\boldsymbol{k}''+2\boldsymbol{k_1})\cdot\boldsymbol{l}''} \\ & \quad \times \sum_{ll'} A_{ll'l''jj'j''\alpha\beta\gamma} \mathrm{e}^{-\mathrm{i}\boldsymbol{k_1}(l-l'')} \mathrm{e}^{-\mathrm{i}\boldsymbol{k_1}(l'-l'')}. \end{aligned} \tag{A.11}$$

Similarly in expression $U_1^{\boldsymbol{k_1}\boldsymbol{k_2}}$, if we introduce $\mathrm{e}^{\mathrm{i}(\boldsymbol{k_1}+\boldsymbol{k_2})\cdot\boldsymbol{l}''}$ $\mathrm{e}^{-(\boldsymbol{k_1}+\boldsymbol{k_2})\cdot\boldsymbol{l}''} = 1$ and $\mathrm{e}^{\mathrm{i}(\boldsymbol{k_1}-\boldsymbol{k_2})\cdot\boldsymbol{l}''} \mathrm{e}^{-\mathrm{i}(\boldsymbol{k_1}-\boldsymbol{k_2})\cdot\boldsymbol{l}''} = 1$, the first of the four terms becomes:

$$\begin{aligned} & \sum_{\boldsymbol{k}''} \sum_{jj'j''} \sum_{\alpha\beta\gamma} m_{j\alpha}^{\boldsymbol{k_1}} m_{j'\beta}^{\boldsymbol{k_2}} u_{j''\gamma}^{\boldsymbol{k}''} \sum_{l''} \mathrm{e}^{-\mathrm{i}(\boldsymbol{k}''+\boldsymbol{k_1}+\boldsymbol{k_2})\cdot\boldsymbol{l}''} \\ & \quad \times \sum_{ll'} A_{ll'l''jj'j''\alpha\beta\gamma} \mathrm{e}^{-\mathrm{i}\boldsymbol{k_1}(l-l'')} \mathrm{e}^{-\mathrm{i}\boldsymbol{k_2}(l'-l'')}. \end{aligned} \tag{A.12}$$

The last sums $\sum_{ll'}$ correspond to double Fourier transforms and can be expressed as:

$$B_{jj'j''\alpha\beta\gamma}(\boldsymbol{k_1}) = \sum_{ll'} A_{ll'l''jj'j''\alpha\beta\gamma} \mathrm{e}^{-\mathrm{i}\boldsymbol{k_1}(l-l'')} \mathrm{e}^{-\mathrm{i}\boldsymbol{k_1}(l'-l'')} \tag{A.13}$$

and

$$C_{jj'j''\alpha\beta\gamma}(\boldsymbol{k_1}, \boldsymbol{k_2}) = \sum_{ll'} A_{ll'l''jj'j''\alpha\beta\gamma} \mathrm{e}^{-\mathrm{i}\boldsymbol{k_1}(l-l'')} \mathrm{e}^{-\mathrm{i}\boldsymbol{k_2}(l'-l'')} \tag{A.14}$$

quantities which are independent of $\boldsymbol{l}''$, but $B_{jj'j''\alpha\beta\gamma}(\boldsymbol{k_1})$ is a function of the propagation vector $\boldsymbol{k_1}$ whereas $C_{jj'j''\alpha\beta\gamma}(\boldsymbol{k_1}, \boldsymbol{k_2})$ depends on the two propagation vectors $\boldsymbol{k_1}$ and $\boldsymbol{k_2}$.

$U_1^{k_1k_1}$ then reduces to three terms:

$$U_1^{k_1k_1} = \sum_{k''}\sum_{jj'j''}\sum_{\alpha\beta\gamma} B_{jj'j''\alpha\beta\gamma}(\boldsymbol{k_1}) \times \left\{ m_{j\alpha}^{k_1} m_{j'\beta}^{k_1} u_{j''\gamma}^{k''} \sum_{l''} \mathrm{e}^{-\mathrm{i}(\boldsymbol{k''}+2\boldsymbol{k_1})\cdot\boldsymbol{l''}} + m_{j\alpha}^{-k_1} m_{j'\beta}^{-k_1} u_{j''\gamma}^{k''} \sum_{l''} \mathrm{e}^{-\mathrm{i}(\boldsymbol{k''}-2\boldsymbol{k_1})\cdot\boldsymbol{l''}} + (m_{j\alpha}^{k_1} m_{j'\beta}^{-k_1} + m_{j\alpha}^{-k_1} m_{j'\beta}^{k_1}) u_{j''\gamma}^{k''} \sum_{l''} \mathrm{e}^{-\mathrm{i}\boldsymbol{k''}\cdot\boldsymbol{l''}} \right\} \quad \text{(A.15)}$$

and $U_1^{k_1k_2}$ is composed of four terms:

$$U_1^{k_1k_2} = \sum_{k''}\sum_{jj'j''}\sum_{\alpha\beta\gamma} C_{jj'j''\alpha\beta\gamma}(\boldsymbol{k_1}, \boldsymbol{k_2}) \times \left\{ m_{j\alpha}^{k_1} m_{j'\beta}^{k_2} u_{j''\gamma}^{k''} \sum_{l''} \mathrm{e}^{-\mathrm{i}(\boldsymbol{k''}+\boldsymbol{k_1}+\boldsymbol{k_2})\cdot\boldsymbol{l''}} + m_{j\alpha}^{-k_1} m_{j'\beta}^{-k_2} u_{j''\gamma}^{k''} \sum_{l''} \mathrm{e}^{-\mathrm{i}(\boldsymbol{k''}-\boldsymbol{k_1}-\boldsymbol{k_2})\cdot\boldsymbol{l''}} + m_{j\alpha}^{k_1} m_{j'\beta}^{-k_2} u_{j''\gamma}^{k''} \sum_{l''} \mathrm{e}^{-\mathrm{i}(\boldsymbol{k''}+\boldsymbol{k_1}-\boldsymbol{k_2})\cdot\boldsymbol{l''}} + m_{j\alpha}^{-k_1} m_{j'\beta}^{k_2} u_{j''\gamma}^{k''} \sum_{l''} \mathrm{e}^{-\mathrm{i}(\boldsymbol{k''}-\boldsymbol{k_1}+\boldsymbol{k_2})\cdot\boldsymbol{l''}} \right\}. \quad \text{(A.16)}$$

For interactions involving magnetic components of the same propagation vector, the expression of $U_1^{k_1k_1}$, equation (A.15), shows that the sum over all the nodes of the lattice l'' is zero unless the $\boldsymbol{k}$-space vector in the exponential is a reciprocal lattice vector, which means inside the first Brillouin zone:

$$\boldsymbol{k''} = \pm 2\boldsymbol{k_1} \text{ for the first two terms}$$

$$\boldsymbol{k''} = 0 \text{ for the third term.}$$

For interactions involving magnetic components of the different propagation vectors ($U_1^{k_1k_2}$, equation (A.16)), the sum over all the nodes of the lattice l" is zero unless:

$$\boldsymbol{k''} = \pm(\boldsymbol{k_1} + \boldsymbol{k_2}) \text{ for the first two terms}$$

$$\boldsymbol{k''} = \pm(\boldsymbol{k_1} - \boldsymbol{k_2}) \text{ for the last two terms.}$$

One should also consider the other fourth order terms, which are either purely magnetic, and fourth order in $\boldsymbol{m}$, or related to the strain wave only, and quadratic in $\boldsymbol{u}$. As the x-ray diffraction study of the strain wave, section 5, is performed in the non-resonant regime, the purely magnetic terms may be neglected here. The simplest form of quadratic terms in $\boldsymbol{u}$ would be $\boldsymbol{u^k} \cdot \boldsymbol{u^{-k*}}$, which is isotropic and thus does not yield any insight on the symmetry of the problem, which we are investigating. Higher order, anisotropic terms might do that, but are beyond the scope of this work. The components of $u^k u^{*k'}$, which may be seen as frozen zero-energy phonon modes, will also result in scattered intensity at positions $2\boldsymbol{k}$ or $\boldsymbol{k_1} \pm \boldsymbol{k_2}$ in the reciprocal space. This will not alter our conclusions on the existence or not of the satellites resulting from the magneto-elastic interaction, and one should just keep in mind that the calculated displacements may actually be renormalized.

References

[1] Walker M B 1980 *Phys. Rev.* B **22** 1338
[2] Mori M and Tsunoda Y 1993 *J. Phys.: Condens. Matter* **5** L77
[3] Tsunoda Y, Mori M, Kunitomi N, Teraoka Y and Kanamori J 1974 *Solid State Commun.* **14** 287
[4] Eagen C F and Werner S A 1975 *Solid State Commun.* **16** 1113
[5] Hill J P, Helgesen G and Gibbs D 1995 *Phys. Rev.* B **51** 10336
[6] de Oliveira A J A, de Souza P E N, Giles C, Mazzaro I and de Camargo P C 2007 *J. Magn. Magn. Mater.* **310** e316
[7] Kimura T, Ishihara S, Shintani H, Arima T, Takahashi K T, Ishizaka K and Tokura Y 2003 *Phys. Rev.* B **68** 060403
[8] Strempfer J, Bohnenbruck B, Mostovoy M, Aliouane N, Argyriuo D N, Schrettle F, Hemberger J, Krimmel A and Zimmermann M v 2007 *Phys. Rev.* B **75** 212402
[9] Vettier C, de Bergevin F, Bernhoeft N, Stunault A and Wermeille D 1999 *SPIE Conf. Proc.* **3773** 351
[10] Longfield M J, Paixão J A, Bernhoeft N and Lander G H 2002 *Phys. Rev.* B **66** 054417
[11] Barbara B, Boucherle J-X, Buevoz J-L, Rossignol M F and Schweizer J 1977 *Solid State Commun.* **24** 481
Barbara B, Boucherle J-X, Buevoz J-L, Rossignol M F and Schweizer J 1979 *Solid State Commun.* **29** 810 (erratum)
[12] Forgan E M, Rainford B D, Lee S L, Abell J S and Bi Y 1990 *J. Phys.: Condens. Matter* **2** 10211
[13] Givord F, Schweizer J and Tasset F 1997 *Physica* B **234–236** 685
[14] Schweizer J, Givord F, Boucherle J-X, Bourdarot F and Ressouche E 2008 *J. Phys.: Condens. Matter* **20** 135204
[15] Harris A B and Schweizer J 2006 *Phys. Rev.* B **74** 134411
[16] Schweizer J, Villain J and Harris A B 2007 *Eur. Phys. J. Appl. Phys.* **38** 41
[17] Lyubarskii G Ya 1960 *The Applicationof Group Theory in Physics* (New York: Pergamon)
[18] Kovalev O V 1993 *Representations of the Crystallographic Space Groups* 2nd edn, ed H T Stokes and D M Haych (London: Gordon and Breach)
[19] McMorrow D F, Lussier J-G, Lebech B, Sørensen S Aa, Christensen M J and Vogt O 1997 *J. Phys.: Condens. Matter* **9** 1133
[20] Stunault A, Vettier C, Regnault L P, de Bergevin F, Paolasini L and Henry J Y 2004 *Physica* B **345** 74
[21] Janoušová B, Detlefs C, Danis S, Prchal J, Komatsubara T and Sechovský V 2006 *J. Alloys Compounds* **408–412** 33
[22] Paolasini L, Di Matteo S, Deen P P, Wilkins S, Mazzoli C, Detlefs B, Lapertot G and Canfield P 2008 *Phys. Rev.* B **77** 094433
[23] Stunault A, Vettier C, de Bergevin F, Bernhoeft N, Fernandez V, Langridge S, Lidström E, Lorenzo-Diaz J E, Wermeille D, Chabert L and Chagnon R 1998 *J. Synchrotron Radiat.* **5** 1010
[24] Hannon J P, Trammell G T, Blume M and Gibbs D 1988 *Phys. Rev. Lett.* **61** 1245
Hannon J P, Trammell G T, Blume M and Gibbs D 1989 *Phys. Rev. Lett.* **62** 2644 (erratum)
[25] Hamrick M D 1996 *PhD Thesis* Rice University, USA
[26] Hill J P and McMorrow D F 1996 *Acta Crystallogr.* A **52** 236
[27] Lebech B 1995 *Magnetic Neutron Scattering* ed A Furrer (Singapore: World Scientific) p 58
[28] Overhauser A W 1971 *Phys. Rev.* B **3** 3173
[29] Aldhart W 1982 *Acta Crystallogr.* A **38** 498